galaxies

IMPACT FACTOR 2.5

CITESCORE 4.1

Article

A Lepton–Hadron Model for the Multi-Wavelength Emission from Extreme High-Frequency Peaked BL Lacertae 1ES 1218+304

Wenjing Dong, Qian Dong and Yonggang Zheng

MDPI

https://doi.org/10.3390/galaxies12010002

galaxies

MDPI

Article

A Lepton–Hadron Model for the Multi-Wavelength Emission from Extreme High-Frequency Peaked BL Lacertae 1ES 1218+304

Wenjing Dong [1], Qian Dong [2] and Yonggang Zheng [1,*]

[1] Department of Physics, Yunnan Normal University, Kunming 650092, China; 2223090042@ynnu.edu.cn
[2] Department of Astronomy, Xiamen University, Xiamen 361005, China; dongqian1018@stu.xmu.edu.cn
* Correspondence: ynzyg@ynu.edu.cn

Abstract: We develop a lepton–hadron model for the possible origin of hard very high energy (VHE) spectra from a distant blazar. The model includes synchrotron self-Compton (SSC) and hadronic components. The lepton components include synchrotron radiation and inverse Compton scattering of relativistic electrons. For the hadronic components, we consider proton synchrotron radiation and investigate the interaction of protons with the synchrotron emission soft photons or cosmic microwave background (CMB) photons. Upon adopting the parametrization of the observed spectrum of 1ES 1218+304, we obtain the following results: (1) the model is able to match the spectral energy distribution of 1ES 1218+304; (2) we find that in $E_{\rm p} \approx 10^{10} \sim 10^{17}$ eV, the $\pi^0 \rightarrow \gamma$-ray process contributes the majority of the secondary photons; and (3) the interaction of protons with the low-energy photons may occur in or outside the jet.

Keywords: galaxies; BL Lacertae objects; radiation mechanisms; non-thermal; gamma-rays; individual; 1ES 1218+304

Citation: Dong, W.; Dong, Q.; Zheng, Y. A Lepton–Hadron Model for the Multi-Wavelength Emission from Extreme High-Frequency Peaked BL Lacertae 1ES 1218+304. *Galaxies* **2024**, *12*, 2. https://doi.org/10.3390/galaxies12010002

Academic Editor: Bidzina Kapanadze

Received: 30 November 2023
Revised: 21 December 2023
Accepted: 25 December 2023
Published: 29 December 2023

1. Introduction

Blazars are a special class of active galactic nucleus (AGN) with non-thermal emission, which arises from the relativistic jet aligned to the observer's line of sight. Blazars are often classified according to their emission lines as BL Lacertae objects (BL Lacs) or flat-spectrum radio quasars (FSRQs). BL Lacs have weak or no emission lines, whereas FSRQs have strong emission lines [1,2]. Starting from *Fermi*-LAT and Air Cherenkov telescopes data, one may obtain the spectral energy distribution (SED) from radio to the TeV γ-ray bands. Those $\log \nu - \log \nu F_\nu$ spectra exhibit two clear humps which correspond to two different emission mechanisms. The low-energy hump from radio to the soft X-ray bands [3] may be ascribed to synchrotron radiation of relativistic electrons [4], whereas the emission mechanism behind the high-energy hump is still disputed. The leptonic model argues that the high-energy hump from hard X-ray to TeV γ-ray corresponds to radiation generated by inverse Compton (IC) scattering of relativistic electrons. This includes synchrotron self-Compton (SSC) and external Compton (EC) contributions according to their soft photons' origin [5]. The SSC model considers the soft photons from synchrotron photons in the jet [6–8], whereas the EC model ascribes those soft photons to the disk [5,9], broad-line region [5,10–12], and dusty molecular torus (MT) [13]. The hadronic model argues that the high-energy hump is due to proton synchrotron emission [14,15] or meson generated by the proton–photon interaction [15–17].

BL Lac objects are classified into four categories according to the magnitude of the synchrotron peak frequency v^{syn}_{peak} : $v^{syn}_{peak} < 10^{14}$ Hz is called Low peaked BL Lacs (LBL), 10^{14} Hz $\leq v^{syn}_{peak} < 10^{15}$ Hz is called Intermediate peaked BL Lacs (IBL), 10^{15} Hz $\leq v^{syn}_{peak} < 10^{17}$ Hz is called High peaked BL Lacs (HBL), and 10^{17} Hz $\leq v^{syn}_{peak}$ are called extreme high peaked BL Lacs (EHBLs) [18,19].

In the standard SSC model view, the synchrotron radiation peak located in the X-ray band pushes the second peak into the very high-energy γ-ray band (VHE, energies above 100 GeV). Observations have shown, however, that in some objects the second peak actually moves at higher energies—above the TeV γ-ray region—making their SED a challenge for the standard lepton SSC model. Indeed, in this case, the decrease in the scattering cross section with energy in the Klein–Nishina system will inevitably lead to quite soft SSC spectra at TeV energies, contrary to observations [19,20].

Observations of very-high-energy (VHE) γ-rays have shown that more than 40 blazars radiate γ-rays in the TeV energy region [21,22]. It has been suggested that primary TeV photons from distant TeV blazars produce electron–positron pairs due to interactions with the extragalactic background light (EBL) [23]. However, the observed spectra do not show a sharp cutoff at energies around 1 TeV [24,25]. A typical example is the VHE γ-ray emission in the distant blazar 1ES 1101-232, which was detected by the High Energy Stereo System (H.E.S.S.) of the Cherenkov Telescope Array [24,26]. The VHE γ-ray data result in very hard intrinsic spectra, with a peak above 3 TeV in the SED, corrected for EBL absorption at the lowest energy level [26]. Similar behavior has been detected in other TeV blazars such as 1ES 0229+200 [27], 1ES 0347-121 [28], and Mkn 501 [29]. EHBLs do not show as high and fast variability as other blazars like HBLs (e.g., low variability of 1ES 0229+200 in the long-term light curve of VHE γ-rays in [30]). This effect may be related to the low flux of these sources, but lepton models predict large flux variations that have never been observed on short time scales. The hard VHE γ-ray spectrum and the absence of fast flux variability make EHBLs interesting candidates for hadronic and lepton–hadronic emission models, which can reproduce their observed SEDs well [19,31].

For the hard spectrum of EHBLs at ultra-high γ-ray energies, the SSC model [32] is unable to explain the ultra-high γ-ray energy emission. Therefore, different emission mechanisms have been proposed to explain this spectral region, and Murase et al. [33] proposed that the interaction of very high-energy photons with EBL photons produces $e^{\pm}$, and the resulting $e^{\pm}$ can IC high-energy photons to higher energies. In addition, Murase et al. [33] considered that cascade emission induced by ultra-high energy cosmic rays could also lead to emission in the high-energy region of the spectrum. Lefa et al. [34] explored lepton models, namely the single-region SSC and EC scenarios, to see if they could account for hard γ spectra with a narrow distribution of energetic particles. On the other hand, Simet et al. [35] proposed the existence of axion-like particles, while Protheroe and Meyer [36] argued for Lorentz invariance violation as the origin of the hard spectrum. The surprisingly low attenuation of high-energy γ-rays, and in particular the shape of the VHE γ-ray tails in the observed spectra, can be explained by secondary γ-rays produced in interstellar space by the interaction of cosmic ray protons with background photons [37–40]. Hard spectra are expected if γ-rays from distant blazars consist mainly of secondary γ-rays that are produced along the line of sight by the interaction of cosmic ray protons with background photons [37–39]. 1ES 0229+200 is one of the most-studied EHBLs detected by TeV γ-rays, and hard TeV spectra in intergalactic cascade scenarios have been successfully interpreted in [33]. Dong et al. [41] researched the accelerated protons in the jet's interaction with cosmic microwave background (CMB) photons to produce electron pairs, which in turn form cascading spectra by IC scattering of these electron pairs with soft photons.

However, due to the lack of extreme high-energy data, it has not been possible to estimate suitable parameters to fit the TeV spectra based on different models. More data are now available to study the nature of γ-rays, and some of the data from EHBLs can be accessed. Here, we focus on investigating the detailed properties of the previously known TeV emitter 1ES 1218+304. In this framework, we use a lepton–hadron model to derive the SED of EHBL and then explore their radiation mechanisms by varying the free parameters to fit the SED to the observed data.

This paper is structured as follows. In Section 2, we present a detailed description of our model. In Section 3, we apply our model to the BL Lac 1ES 1218+304. In Section 4, we discuss results and in Section 5 we close the paper with some concluding remarks.

Throughout the paper, we assume the Hubble constant $H_0 = 75$ km s^{-1} Mpc^{-1}, the dimensionless cosmological constant $\Omega_\Lambda = 0.73$, matter energy density $\Omega_M = 0.27$, and radiation energy density $\Omega_R = 0$ [42].

2. The Model

We assume that the radiating region is homogeneously spherical. We consider the lepton–hadron model, i.e., SSC and hadron processes. For the lepton components, including synchrotron radiation and inverse Compton scattering of relativistic electrons, the hadronic components contain both the synchrotron radiation of protons and the proton–photon process. For the proton–photon process, we use the method in [42,43] to obtain the secondary γ-ray components. We use the method in [41,42] to calculate the Bethe–Heitler process.

2.1. SSC Component

We assume that the electron distribution $N_e(\gamma_e)$ in the jet follows a broken power-law distribution governed by the electron spectral index n_1, n_2 as follows:

$$N_e(\gamma_e) = \begin{cases} N_{e,0}\gamma_e^{-n_1}, & \gamma_{e,\min} \le \gamma_e \le \gamma_{e,b} \\ N_{e,1}\gamma_e^{-n_2}, & \gamma_{e,b} \le \gamma_e \le \gamma_{e,cut} \end{cases} \quad (1)$$

where $\gamma_{e,min}$, $\gamma_{e,b}$, and $\gamma_{e,cut}$ are the minimum Lorentz factor, broken Lorentz factor, and cutoff Lorentz factor, respectively. It is easy to obtain the relation $N_{e,1} = N_{e,0}\gamma_{e,b}^{(n_2-n_1)}$ when $\gamma_e = \gamma_{e,b}$. In the source coordinate system, we get the synchrotron radiation intensity $I_{syn}(\nu)$ [7] through the radiation transfer equation and calculate the IC intensity $I_{Ic}(\nu)$ using the differential photon production rate [44,45]. The emission blob moves relativistically with respect to the observer, and the observed emission intensity in the laboratory coordinate system is enhanced by the Doppler beaming effect [1]. Therefore, considering the Doppler beaming correction, the emission flux in the observer coordinate system may be expressed as

$$\frac{dN_\gamma^{\rm int}}{dE_\gamma} = \pi \frac{{r_1}^2}{d^2 E_\gamma^2} \delta^3 (1+z) \left[I_{syn}(E_\gamma) + I_{Ic}(E_\gamma) \right] \quad (2)$$

where r_1 and d are the radius of the emission blob and luminosity distances, respectively. z is the red shift and $\delta = [\Gamma(1 - \beta cos\theta)]^{-1}$ is the Doppler factor which depends on the blob Lorentz factor Γ and the angle θ between the moving direction of the emission blob and the observer's line of sight. Additionally, taking account of the EBL absorption, i.e., the interaction of very high-energy photons with the EBL photons, we have [46–50],

$$\frac{dN_\gamma^{obs}}{dE_\gamma} = \frac{dN_\gamma^{\rm int}}{dE_\gamma} \exp[-\tau(E_{\gamma,z})] \quad (3)$$

where $\tau(E_\gamma, z)$ is the absorption optical depth, and we adopt its corresponding EBL model in [51].

2.2. Hadronic Component

The synchrotron radiation of protons is analogous to the synchrotron radiation of electrons, which just replaces the mass of the electron with the mass of the proton in Section 2.1. For the Bethe–Heitler process, we refer to the method in [42] for calculation which describe the secondary γ-ray production rate clearly. Additionally, the interaction of relativistic protons with low-energy photons may produce π^0 and $\pi^\pm$ mesons according to

$$p + \gamma \to n_0\pi^0 + n_+\pi^+ + n_-\pi^- + ... \quad (4)$$

where n_0, n_+ and n_- represent the number of mesons (we assume their values are all one). We assume that the low-energy photons originate from the synchrotron photons or

CMB photons. For synchronous soft photons, we assume an energy threshold for photons as follows:

$$\epsilon \ll m_\pi c^2 \tag{5}$$

where ϵ is the energy of photons, and m_π is the mass of π meson. For CMB photons, the distribution $N_{\rm ph}(E_s)$ satisfies the following equation:

$$N_{\rm ph}(E_s) = \frac{1}{\pi^2(hc)^3}\frac{E_s^2}{\exp(E_s/kT)-1} \tag{6}$$

where E_s is the CMB photons' energy and the CMB temperature $T = 2.73 \times (1+z)$K with Boltzmann constant $k = 1.38 \times 10^{-16}$ erg/K and Planck constant $h = 6.63 \times 10^{-27}\ erg \cdot s$. The frequency range of the CMB is $3 \times 10^8 \sim 3 \times 10^{19}$ Hz. Moreover, we assume that the proton distribution in the jet displays a power-law distribution with a high-energy cutoff,

$$N_p(E_p) = N_{p,0} e^{-\frac{E_p}{E_{p,max}}} E_p^{-\alpha} \tag{7}$$

$N_{p,0}$ is a normalization coefficient, E_p represents the energy of protons, and α is the proton spectral index. The production rate of γ-rays is given by [43]

$$\frac{dN_\gamma}{dE_\gamma} = \frac{m_p^2c^4}{4}\int_{\eta_0}^{\infty}\int_{E_\gamma}^{\infty}\frac{dE_p}{E_p^2}N_p(E_p) \times f_{ph}(\frac{\eta m_p^2c^4}{4E_p})\Phi_\gamma(\eta, x)d\eta \tag{8}$$

where $\eta_0 = 2\frac{m_\pi}{m_p} + \frac{m_\pi^2}{m_p^2}$ and $\eta = \frac{4\epsilon E_p}{m_p^2c^4} \geq \eta_0$, c is the light speed, the energy of photons can be expressed as $\epsilon = \frac{\eta m_p^2c^4}{4E_p}$ and $f_{ph}(\frac{\eta m_p^2c^4}{4E_p})$ describes the density of the low-energy photons. E_γ is the energy of γ-ray and $\Phi_\gamma(\eta, x)$ represents its distribution which depends on η and $x = \frac{E_\gamma}{E_p}$ as follows [43,52]:

$$\Phi_\gamma(\eta, x) = \begin{cases} B_\gamma(ln2)^\psi, & x < x_- \\ B_\gamma exp\left\{-s_\gamma[ln(\frac{x}{x_-})]^{\delta_\gamma}\right\} \times [ln(\frac{2}{1+y^2})]^\psi, & x_- < x < x_+ \\ 0, & x > x_+ \end{cases} \tag{9}$$

with $y = \frac{x-x_-}{x_+-x_-}$, $\psi = 2.5 + 0.4ln(\frac{\eta}{\eta_0})$, B_γ, s_γ, δ_γ fitted using Table I of in [43]. In addition, Kelner and Aharonian also define the quantity $x_\pm$ [43],

$$x_\pm = \frac{1}{2(1+\eta)}[\eta + r^2 \pm \sqrt{(\eta - r^2 - 2r)(\eta - r^2 + 2r)}], \tag{10}$$

where $r = \frac{m_\pi}{m_p}$.

3. Application of the Model to 1ES 1218+304

The redshift z = 0.182 for 1ES 1218+304 was determined in 1997 using the spectroscopic measurements of the host galaxy [53]. 1ES 1218+304 has been first observed by Major Atmospheric Gamma Imaging Cherenkov (MAGIC) at VHE [54] and then through the Very Energetic Radiation Imaging Telescope Array System (VERITAS) [55]. The *Fermi*-Large Area Telescope (*Fermi*-LAT) continuously monitors the HE γ-ray radiation from 1ES 1218+304 and lists it in its continuous catalogue as one of the hardest blazars above 0.10 GeV [56–58]. Its hard VHE γ-ray spectrum from MeV/GeV to TeV bands means that the emission is most likely to be produced by fresh accelerated electrons, allowing the various acceleration and cooling processes of the emitted particles to be tested [59].

We use the available multi-wavelength (non-simultaneous) archival data from the ASI Science Data Center (SSDC) compiled by Foffano et al. [19] (the archival data contains

multi-wavelength spectra from the radio band to the γ-ray. One obtains radio bands from the NVSS points [60], infrared bands from *WISE* points, optical to ultraviolet from *Swift*-UVOT [61] points, soft X-ray bands from the *Swift*-XRT [62] or from *Beppo*-SAX data, and hard X-rays from *Swift*-BAT 105 months [63]. Additionally, we have information about high-energy γ-ray bands from ten years of *Fermi*-LAT data [19].) and hard X-ray data from *Swift* available on SSDC. Using the model in Section 2, we can calculate the TeV γ-ray spectra, then the hard intrinsic spectrum of the source can be produced. The two origins of the γ-photon will be considered separately.

We apply our model to generate the SED, and in the case of two soft photons, the parameters of the obtained SSC part are the same, and we assume that there is a broken power law for the high-energy electron distribution between $\gamma_{e,min} = 200.00$ and $\gamma_{e,cut} = 1.00 \times 10^8$ [41] with a break at $\gamma_{e,b} = 8.20 \times 10^4$. The density normalization is $N_{e,0} = 9.60 \times 10^2$ cm^{-3}, the energy index of the particles between $\gamma_{e,min}$ and $\gamma_{e,b}$ is set to $n_1 = 2.05$, the energy index of the particles between $\gamma_{e,b}$ and $\gamma_{e,cut}$ is set to $n_2 = 4.25$, the magnetic field strength is $B = 0.16$ G, the Doppler factor is $\delta = 20.00$ [64], and the emission blob size r_1 is 2.30×10^{16} cm. The Doppler factor and magnetic strength of the second radiation region are the same as those of the first radiation region. For the two soft photons in the second region, the parameters obtained from the model fitting are as follows: the radii of the emission blob are, respectively, $r_{2,syn} = 4.62 \times 10^{17}$ cm, $r_{2,CMB} = 1.39 \times 10^{18}$ cm, and assume a power-law distribution from $E_{p,min,syn} = 1.40 \times 10^{11}$ eV to $E_{p,max,syn} = 3.39 \times 10^{15}$ eV, $E_{p,min,CMB} = 7.22 \times 10^{10}$ eV to $E_{p,max,CMB} = 1.02 \times 10^{17}$ eV with high-energy cutoff in the high energy, and obtain a spectral index $\alpha_{syn} = 2.30$, $\alpha_{CMB} = 2.00$ and a normalization coefficient $N_{p,0,syn} = 2.26 \times 10^{-8}$ erg^{-1} cm^{-3}, $N_{p,0,CMB} = 2.25 \times 10^{-8}$ erg^{-1} cm^{-3}. The physical parameters of the hadronic components are listed in Table 1. Then, we calculate the multi-wavelength spectrum using our model and find that the TeV γ-ray spectrum is due to the interaction of protons with synchrotron radiation photons or CMB photons. In Figure 1, we show the multi-wavelength spectrum from the X-ray to the TeV γ-ray bands.

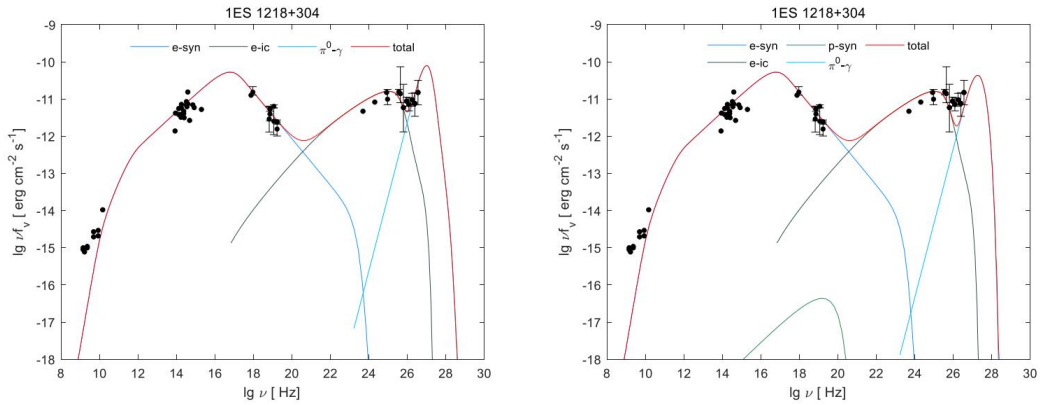

Figure 1. The photons of proton–photon interaction are synchrotron radiation photons (**left** panel) and CMB photons (**right** panel), and the predicted 1ES 1218+304 multi-wavelength spectrum is compared with the observation data. Observations from [19] and hard X-ray data from *Swift* are available on SSDC. Observations are represented by black dots. We employ the solid line to denote the multi-wavelength spectrum with different colors. For the multi-wavelength SED, the dodger-blue solid curve and dark-slate-gray solid curve represents the synchrotron radiation and IC scattering of electrons, respectively. Finally, the sea-green solid curve represents the synchrotron radiation of protons and the deep-sky-blue curve expresses the γ-rays generated from the decay of π^0, whereas the red solid curve denotes the total SED of photons.

Table 1. Physical parameters of the hadronic component.

Parameter	Synchrotron Radiation Soft Photons	CMB Photons
$E_{p,min}$ [eV]	1.40×10^{11}	7.22×10^{10}
$E_{p,max}$ [eV]	3.39×10^{15}	1.02×10^{17}
$N_{p,0}$ [erg^{-1}cm^{-3}]	2.26×10^{-8}	2.25×10^{-8}
α	2.30	2.00
r_2 [cm]	4.62×10^{17}	1.39×10^{18}

4. Discussion and Conclusions

In this paper, our model predicts a γ-ray spectrum in the VHE band with an energy peak above $\sim$ TeV, consistent with the observations. We have discussed the interaction of protons with low-energy photons from the synchrotron radiation of blazar 1ES 1218+304 or CMB photons. The lepton components contribute two peaks from the radio band to the γ-ray band. The related hadronic components also contribute to the multi-wavelength spectrum: the synchrotron emission and IC emission of Bethe–Heitler pairs contribute very minimally, not drawn in the figure, that the proton synchrotron radiation has a partial contribution in the case of CMB for soft photons, and the decay of π^0 affects the γ-rays.

4.1. Power-Law Proton Distribution

Blazars are a special class of the AGN with the jet which contains large and significant information about the physical process. Those physical processes include the injection, acceleration, cooling, and escape, and shape the electron energy distribution. In the case of non-relativistic and parallel excitations, we assume a monoenergetic injection upstream, and if the size of the shocked flow is limitless, we can obtain a power-law electron energy distribution in the downstream flow [65,66]. Generally, the estimation of the acceleration timescales in valid magnetic magnitude is $t_{acc} \sim 3\kappa/u_s^2$, u_s is the velocity of the shock in the upstream coordinate system and κ expresses the spatial diffusion coefficient [67]. In the condition of the Bohm limit, the average free path λ of particles is equal to the their gyro-radius r_g, $\Delta B \leq B$ (Δ is the degree of change of the magnetic field) and $\kappa \leq \kappa_B = r_g c/3$, so

$$t_{acc} \leq \frac{\gamma_p m_p c}{eB}(\frac{c}{u_s})^2 = \frac{r_g c}{u_s^2} \tag{11}$$

In the case of low-energy photons being synchrotron radiation soft photons or CMB photons, we assume that the protons are accelerated to 3.39×10^{15} eV, 1.02×10^{17} eV by the non-relativistic diffusive shock acceleration with $u_s = 0.1c$, respectively. The calculated radii of the acceleration region are about $R_{acc,syn} = 2.12 \times 10^{16}$ cm, $R_{acc,CMB} = 6.38 \times 10^{17}$ cm. The maximum Larmor radii is described as $R_L = E_{p,max,syn}/(eB) = 7.07 \times 10^{13}$ cm, $R_L = E_{p,max,CMB}/(eB) = 2.13 \times 10^{15}$cm for protons, which is less than the acceleration region. The distribution of the protons haves a high-energy cutoff $E_{p,max}$ and in the timescale of the cooling,

$$\tau_{syn} = \frac{3m_p c}{4\sigma_T u_B}\gamma_p^{-1} \tag{12}$$

From $R_{syn} = \tau_{syn} \times c$, we determine that the dissipation regions are about 4.61×10^{17} cm, 1.53×10^{16} cm. Since both the acceleration region and the dissipation region are smaller than the radius r_2 of the proton emission blob, it is reasonable to assume a power-law distribution with a cutoff.

4.2. $p\gamma \to \pi$

It is an open question whether the p-p process [68,69] is relevant for blazars, i.e., it may lead to γ-ray production. In fact, the condition of a very high-energy density cloud is difficult to achieve in blazars, and the process is usually neglected [41]. Additionally, pions

produced by the interaction of protons with low-energy photons are known to generate extreme high-energy γ-rays outside the jet. The model considers SSC, the γ-ray photon spectrum, cascade pairs resulting from pγ interactions, and proton synchrotron radiation. Pπ process $E_\gamma \sim 0.1E_p$ [40], the proton energy in this paper, is about $E_p \sim 10^1 - 10^8$ GeV. Based on this energy, the energy range of γ-rays produced by the pπ process is about $E_\gamma \sim 1 - 10^7$ GeV. The energy segments considered in this paper cover this range. Concerning the decay of $\pi^\pm$, we leave the discussion for the future, and just note the relationship with neutrino data collected by IceCube [70].

4.3. The Free-Path of the Photomeson Process

In our model, protons mainly lose energy by interacting with the synchrotron emission photons or CMB photons. For the process of proton–photon interaction, the energy loss rate $t_{p\pi}^{-1}$ can be estimated in the proton's rest frame using the following formula [71,72]:

$$t_{p\pi}^{-1}(\gamma_p) = \frac{c}{2\gamma_p^2}\int_{\bar{\epsilon}_{th}}^{\infty}\bar{\epsilon}\sigma_{p\pi}(\bar{\epsilon})\kappa_p(\bar{\epsilon})d\bar{\epsilon}\int_{\epsilon_s^{'}}^{\infty}\frac{n^{'}(\epsilon^{'})}{\epsilon^{'2}}d\epsilon^{'} \tag{13}$$

where $\bar{\epsilon} = 2\gamma_p\epsilon_s^{'}$ and $\epsilon^{'}$ are the energy of soft photons in the proton's rest frame, $\gamma_p = E_p/(m_pc^2)$ is the Lorentz factor of protons, $\epsilon_s^{'} \approx h \times \nu_s$ where $\nu_s \sim 10^{17}$ Hz is the peak frequency of synchrotron emission, and $n^{'}(\epsilon^{'})$ is the photon number density in the co-moving frame of the emission region. For the proton–photon process, $\sigma_{p\pi}(\bar{\epsilon})$ and $\kappa_p(\bar{\epsilon})$ express the photomeson cross-section and proton inelasticity, and imply the threshold value $\bar{\epsilon}_{th} = 145$ MeV. We are just trying to obtain an estimate, so we assume the approximate value $< \sigma_{p\pi}(\bar{\epsilon})\kappa_p(\bar{\epsilon}) > \sim 0.70 \times 10^{-28}$ cm^2 integrate over the entire wavelength range [73,74]. Thus, for the case where the soft photons are synchrotron radiation photons or CMB photons during the proton–photon interaction of 1ES 1218+304, the maximum cooling times are, respectively, $t_{p\pi,syn} \approx 3.42 \times 10^{13}$ s, $t_{p\pi,CMB} \approx 3.25 \times 10^{13}$ s, which corresponds to a travel path $l_{p\pi,syn} \approx 1.02 \times 10^{24}$ cm, $l_{p\pi,CMB} \approx 9.74 \times 10^{23}$ cm. The different travel paths may be mainly due to the different frequency ranges of soft photons.

In this paper, the emission region r_2 is lesser than the free-path of the photomeson process $l_{p\pi}$. For this, we give a thought to the total efficiency of the total process which is expressed by $\eta_{p\pi}$ [75] as follows:

$$\eta_{p\pi} = \frac{\int_{\gamma_{p,min}}^{\gamma_{p,max}}\tau_{p\pi}N_p(E_p)\gamma_p d\gamma_p}{\int_{\gamma_{p,min}}^{\gamma_{p,max}}N_p(E_p)\gamma_p d\gamma_p} \tag{14}$$

where the opacity of the photon–meson process expressed as $\tau_{p\pi}(\gamma_p) = t_{p\pi}(\gamma_p)^{-1}/t_{dyn}^{-1}$ and $t_{dyn} = r_2/c$ is the dynamical timescale in the co-moving coordinates system. Actually, the effective rate under this circumstance is approximately 0.06 and 0.04, respectively, and the difference may be due to the fact that the synchrotron soft photon density is greater than the CMB photon density. We used averaged state data and did not compare variable timescales with observation timescales, which can be considered later in the work.

4.4. The Contribution to the Total Spectrum

Whether it is synchronous soft photons or CMB photons, BH-ic's and BH-syn's contribution to the total spectrum are small. Proton synchrotron radiation has a larger frequency range and a slightly stronger contribution when CMB photons are soft photons, whereas the opposite is true of $\pi^0 \rightarrow \gamma$. The coordinates of the third peak are, respectively, (27.01, -10.10) and (27.24, -10.36). From Figure 2, we can see that there is a difference in the γ-rays from the two soft photons. Before, $logv \approx 27.26$ Hz synchrotron soft photons correspond to a larger flux at the same frequency, and after $logv \approx 27.26$ Hz, the opposite is true.

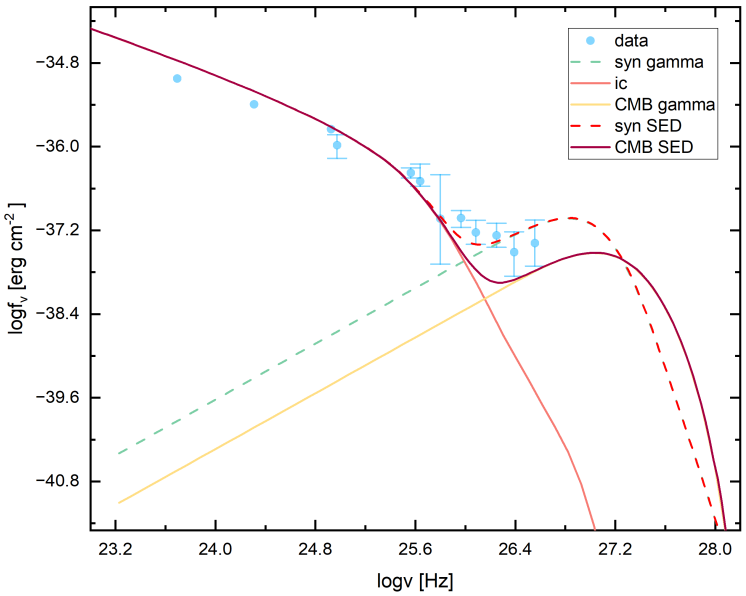

Figure 2. Comparison of the $\pi^0 \rightarrow$ γ-ray patterns of the two soft photons in the pγ process. The observed data points are represented by blue dots, the IC is represented by a pink solid line. When the soft photon is the synchrotron radiation photon, the gamma rays and total flux are represented by the light green dashed line and the red dotted line, respectively. For the soft photon is the CMB photon, the gamma rays and total flux are represented by the yellow solid line and dark red solid line, respectively.

The flux of the primary γ-rays is attenuated by their interactions with the EBL. For a source at distance, the flux of unattenuated high-energy gamma rays is

$$F_{\text{primary},\gamma}(d) \propto \frac{1}{d^2} \exp\{-d/\lambda_\gamma\}, \tag{15}$$

For the flux per unit area $F_{\text{secondary, }\gamma}(d) = \frac{\Phi_\gamma(d)}{(4\pi d^2)}$, this solution gives

$$F_{\text{secondary},\gamma}(d) = \frac{p\lambda_\gamma}{4\pi d^2}[1 - e^{-d/\lambda_\gamma}] \propto \begin{cases} 1/d, & \text{d} \ll \lambda_\gamma, \\ 1/d^2, & \text{d} \gg \lambda_\gamma. \end{cases} \tag{16}$$

It is clear from Equations (15) and (16) that for a sufficiently high proton flux, secondary gamma rays should dominate the spectrum of very distant sources above E $\sim$ TeV, since their flux suppression is less severe at large distances [39].

4.5. Luminosity Estimates

Assuming that the jet is made of a plasma of electrons and protons, the jet kinetic power L_{kin} [76] can be expressed as $L_{kin} \approx L_e + L_p + L_B$ in the stationary frame of the host galaxy [77–83]. The electron power L_e is characterized by the energy density $u_e^{'} = m_e c^2 \int_{\gamma_{e,min}}^{\gamma_{e,max}} N_e(\gamma_e)\gamma_e d\gamma_e$ in the co-moving frame where the bulk Lorentz factor Γ_b is approximated by δ when the angle between the sight of observer line and the jet axis is about $\frac{1}{\Gamma_b}$,

$$L_e = \pi {r_1}^2 \Gamma_b^2 c u_e^{'} \tag{17}$$

For the proton power L_p,

$$L_p = \pi {r_2}^2 \Gamma_b^2 c u_p^{'} \tag{18}$$

and the energy density of protons is expressed by $u_p^{'} = \int_{E_{p,min}}^{E_{p,max}} N_p(E_p) E_p dE_p$. Additionally, the power of magnetic field L_B may be calculated as

$$L_B = \frac{1}{8} r_2{}^2 \Gamma_b^2 c B^2. \quad (19)$$

According to the above calculation, jet kinetic power in the case of low-energy soft photons from electron–synchrotron radiation is $L_{kin,syn} \approx 6.44 \times 10^{43} + 9.37 \times 10^{41} + 8.19 \times 10^{45} \approx 8.26 \times 10^{45}$ erg s^{-1}. In the case where the CMB photon is a low-energy soft photon, the jet kinetic power is $L_{kin,CMB} \approx 6.44 \times 10^{43} + 2.33 \times 10^{43} + 7.41 \times 10^{46} \approx 7.42 \times 10^{46}$ erg s^{-1}. The electronic power L_e is the same in these two cases, whereas there is a large difference in proton power L_p and the magnetic field power L_B. The super massive black hole (SMBH) mass of BL Lac 1ES 1218+304 is 6×10^8 $M_\odot$ [76] and its Eddington luminosity is $L_{Edd} \simeq 7.5 \times 10^{46}$ erg s^{-1}. The jet kinetic power L_{kin} is less than the Eddington luminosity L_{Edd} and this indicates that the SMBH fully provides the radiation pressure. The background photons like EBL photons also can be used as the seed photons in the galactic space. The wavelength range of EBL photons is approximately $3.00 \times 10^{11} \sim 3.00 \times 10^{15}$ Hz and its distribution may be found in [84]. Zheng and Kang [40] proposed that the protons ($E_p = 4.80 \times 10^8 \sim 3.02 \times 10^{19}$ eV) interact with the background photons out of the emission blob and produce the high-energy γ-rays.

4.6. The Selection of Seed Photons

$p + \gamma_{\rm CMB} \rightarrow p + e^+ + e^-$. Essey et al. [39] have taken into account both of these contributions, and argue that for proton energy $E_p = 1.00 \times 10^{18}$ eV and higher, the Bethe–Heitler pair production of CMB photons contributes a large part of the secondary photons. In this paper $E_p = 7.22 \times 10^{10} \sim 1.02 \times 10^{17}$ eV. In this range, we consider synchrotron radiation soft photons and CMB photons as seed photons. From Figure 3, we can see that when the density of the two soft photons is distributed with energy, the synchrotron soft photon has a wider energy range and greater energy density. From Figure 1, we find that in this proton energy range, the $\pi^0 \rightarrow \gamma$-ray process contributes the majority of the secondary photons.

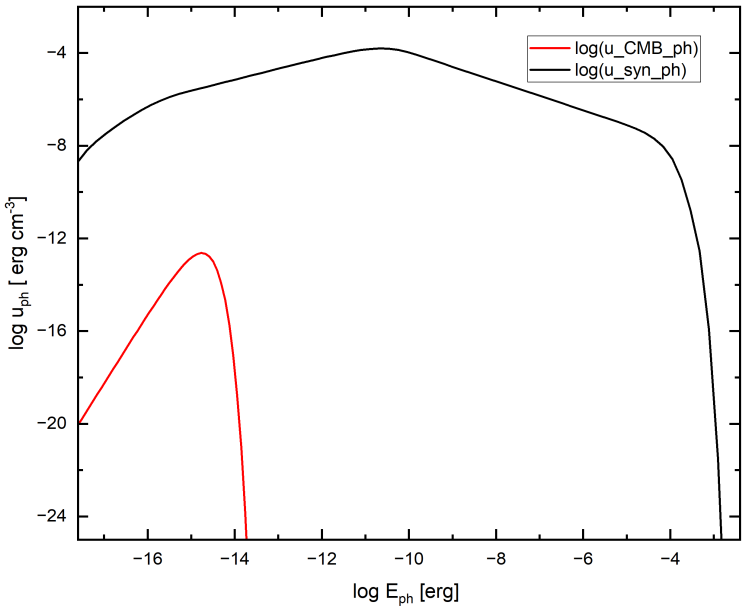

Figure 3. Logarithmic distribution plot of the density of two soft photons as a function of energy, with the red solid line representing the CMB photon and the black solid line representing the synchrotron radiation soft photon.

5. Conclusions

Assuming suitable electron and proton spectra, we obtain satisfactory fits to the observed spectra of distant blazar 1ES 1218+304. This indicates that the very hard intrinsic blazar spectrum in the γ-ray band can be explained by secondary γ-rays produced by the interaction of high-energy protons with synchrotron radiation soft photons or CMB photons in intergalactic space. Our model indicates that (1) the non-relativistic shock acceleration and the synchrotron emission can produce the proton's power-law distribution with high-energy cutoff; (2) if the low-energy soft photons in the proton–photon interaction process are different, the contribution of proton synchrotron radiation and π^0 decay contribute to the total spectrum differently; (3) we find that in $E_p \approx 10^{10} \sim 10^{17}$ eV, the $\pi^0 \rightarrow \gamma$-ray process contributes the majority of the secondary photons; and (4) the parameters of proton spectrum $E_{\rm p,max}$, $E_{\rm p,min}$, $N_{\rm p,0}$, α, the radius r_2 of the proton's emission blob play an important role in determining the proton power, and the radius of the electron radiation zone affects the electronic power. Furthermore, the energetic protons may escape the dissipation region and then interact with the background photons. Perhaps protons interact with proton synchrotron radiation photons in the jet. We leave this issue for the future.

Author Contributions: Formal analysis, W.D.; software, Y.Z.; data curation, W.D.; writing—original draft, W.D. and Q.D.; writing—review and editing, W.D. and Y.Z.; supervision, Y.Z.; funding acquisition, Y.Z. All authors have read and agreed to the published version of the manuscript.

Funding: This work is partially supported by the National Natural Science Foundation of China (grant No. 12363002).

Institutional Review Board Statement: Not applicable.

Informed Consent Statement: Not applicable.

Data Availability Statement: https://tools.ssdc.asi.it/SED/.

Acknowledgments: We acknowledge the use of data, analysis tools, and services from the Open Universe platform, the ASI Space Science Data Center (SSDC), the Astrophysics Science Archive Research Center (HEASARC), Fermi Science Tools, the Astrophysics Data System (ADS), and the National Extra-galactic Database (NED).

Conflicts of Interest: The authors declare no conflicts of interest.

References

1. Urry, C.M.; Padovani, P. Unified Schemes for Radio-Loud Active Galactic Nuclei. *Publ. Astron. Soc. Pac.* **1995**, *107*, 803. [CrossRef]
2. Scarpa, R.; Falomo, R. Are high polarization quasars and BL Lacertae objects really different? A study of the optical spectral properties. *Astron. Astrophys.* **1997**, *325*, 109–123.
3. Costamante, L.; Ghisellini, G.; Giommi, P.; Tagliaferri, G.; Celotti, A.; Chiaberge, M.; Fossati, G.; Maraschi, L.; Tavecchio, F.; Treves, A.; et al. Extreme synchrotron BL Lac objects. Stretching the blazar sequence. *Astron. Astrophys.* **2001**, *371*, 512–526. [CrossRef]
4. Urry, C.M. Multiwavelength properties of blazars. *Adv. Space Res.* **1998**, *21*, 89–100. [CrossRef]
5. Dermer, C.D.; Schlickeiser, R. Model for the High-Energy Emission from Blazars. *Astrophys. J.* **1993**, *416*, 458. [CrossRef]
6. Maraschi, L.; Ghisellini, G.; Celotti, A. A Jet Model for the Gamma-Ray–emitting Blazar 3C 279. *Astrophys. J.* **1992**, *397*, L5. [CrossRef]
7. Bloom, S.D.; Marscher, A.P. An Analysis of the Synchrotron Self-Compton Model for the Multi–Wave Band Spectra of Blazars. *Astrophys. J.* **1996**, *461*, 657. [CrossRef]
8. Mastichiadis, A.; Kirk, J.G. Variability in the synchrotron self-Compton model of blazar emission. *Astron. Astrophys.* **1997**, *320*, 19–25. [CrossRef]
9. Dermer, C.D.; Cerruti, M.; Lott, B.; Boisson, C.; Zech, A. Equipartition Gamma-Ray Blazars and the Location of the Gamma-Ray Emission Site in 3C 279. *Astrophys. J.* **2014**, *782*, 82. [CrossRef]
10. Ghisellini, G.; Madau, P. On the origin of the gamma-ray emission in blazars. *Mon. Not. R. Astron. Soc.* **1996**, *280*, 67–76. [CrossRef]
11. Dermer, C.D.; Schlickeiser, R.; Mastichiadis, A. High-energy gamma radiation from extragalactic radio sources. *Astron. Astrophys.* **1992**, *256*, L27–L30.
12. Sikora, M.; Begelman, M.C.; Rees, M.J. Comptonization of Diffuse Ambient Radiation by a Relativistic Jet: The Source of Gamma Rays from Blazars? *Astrophys. J.* **1994**, *421*, 153. [CrossRef]

13. Błażejowski, M.; Sikora, M.; Moderski, R.; Madejski, G.M. Comptonization of Infrared Radiation from Hot Dust by Relativistic Jets in Quasars. *Astrophys. J.* **2000**, *545*, 107–116. [CrossRef]
14. Aharonian, F.A. TeV gamma rays from BL Lac objects due to synchrotron radiation of extremely high energy protons. *New Astron.* **2000**, *5*, 377–395. [CrossRef]
15. Mücke, A.; Protheroe, R.J. A proton synchrotron blazar model for flaring in Markarian 501. *Astropart. Phys.* **2001**, *15*, 121–136. [CrossRef]
16. Mannheim, K.; Biermann, P.L. Gamma-ray flaring of 3C 279: A proton-initiated cascade in the jet? *Astron. Astrophys.* **1992**, *253*, L21–L24.
17. Mannheim, K. The proton blazar. *Astron. Astrophys.* **1993**, *269*, 67–76. [CrossRef]
18. Mariotti, M. MAGIC discovers VHE gamma-ray emission from the blazar 1ES 1727+502. *Astron. Telegr.* **2011**, *3774*, 1.
19. Foffano, L.; Prandini, E.; Franceschini, A.; Paiano, S. A new hard X-ray-selected sample of extreme high-energy peaked BL Lac objects and their TeV gamma-ray properties. *Mon. Not. R. Astron. Soc.* **2019**, *486*, 1741–1762. [CrossRef]
20. Tavecchio, F.; Ghisellini, G.; Ghirlanda, G.; Costamante, L.; Franceschini, A. The hard TeV spectrum of 1ES 0229+200: New clues from Swift. *Mon. Not. R. Astron. Soc.* **2009**, *399*, L59–L63. [CrossRef]
21. Aharonian, F.; Akhperjanian, A.G.; Bazer-Bachi, A.R.; Beilicke, M.; Benbow, W.; Berge, D.; Bernlöhr, K.; Boisson, C.; Bolz, O.; Borrel, V.; et al. Observations of selected AGN with HESS. *Astron. Astrophys.* **2005**, *441*, 465–472. [CrossRef]
22. Wagner, R.M. Synoptic studies of 17 blazars detected in very high-energy γ-rays. *Mon. Not. R. Astron. Soc.* **2008**, *385*, 119–135. [CrossRef]
23. Gould, R.J.; Schréder, G. Opacity of the Universe to High-Energy Photons. *Phys. Rev. Lett.* **1966**, *16*, 252–254. [CrossRef]
24. Aharonian, F.; Akhperjanian, A.G.; Bazer-Bachi, A.R.; Beilicke, M.; Benbow, W.; Berge, D.; Bernlöhr, K.; Boisson, C.; Bolz, O.; Borrel, V.; et al. Fast Variability of Tera-Electron Volt γ Rays from the Radio Galaxy M87. *Science* **2006**, *314*, 1424–1427. [CrossRef] [PubMed]
25. Acciari, V.A.; Aliu, E.; Arlen, T.; Beilicke, M.; Benbow, W.; Böttcher, M.; Bradbury, S.M.; Buckley, J.H.; Bugaev, V.; Butt, Y.; et al. Veritas Observations of a Very High Energy γ-Ray Flare From the Blazar 3C 66A. *Astrophys. J.* **2009**, *693*, L104–L108. [CrossRef]
26. Aharonian, F.; Akhperjanian, A.G.; Bazer-Bachi, A.R.; Beilicke, M.; Benbow, W.; Berge, D.; Bernlöhr, K.; Boisson, C.; Bolz, O.; Borrel, V.; et al. Detection of VHE gamma-ray emission from the distant blazar 1ES 1101-232 with HESS and broadband characterisation. *Astron. Astrophys.* **2007**, *470*, 475–489. [CrossRef]
27. Aharonian, F.; Akhperjanian, A.G.; Barres de Almeida, U.; Bazer-Bachi, A.R.; Behera, B.; Beilicke, M.; Benbow, W.; Bernlöhr, K.; Boisson, C.; Bolz, O.; et al. New constraints on the mid-IR EBL from the HESS discovery of VHE γ-rays from 1ES 0229+200. *Astron. Astrophys.* **2007**, *475*, L9–L13. [CrossRef]
28. Aharonian, F.; Akhperjanian, A.G.; Barres de Almeida, U.; Bazer-Bachi, A.R.; Behera, B.; Beilicke, M.; Benbow, W.; Bernlöhr, K.; Boisson, C.; Bolz, O.; et al. Discovery of VHE γ-rays from the distant BL Lacertae 1ES 0347-121. *Astron. Astrophys.* **2007**, *473*, L25–L28. [CrossRef]
29. Neronov, A.; Semikoz, D.; Taylor, A.M. Very hard gamma-ray emission from a flare of Mrk 501. *Astron. Astrophys.* **2012**, *541*, A31. [CrossRef]
30. Cologna, G.; Mohamed, M.; Wagner, S.; Wierzcholska, A.; Romoli, C.; Kurtanidze, O. Long term lightcurve of the BL Lac object 1ES 0229+200 at TeV energies. In Proceedings of the 34th International Cosmic Ray Conference (ICRC2015), Hague, The Netherlands, 30 July–6 August 2015; International Cosmic Ray Conference; Volume 34, p. 762. [CrossRef]
31. Cerruti, M.; Zech, A.; Boisson, C.; Inoue, S. A hadronic origin for ultra-high-frequency-peaked BL Lac objects. *Mon. Not. R. Astron. Soc.* **2015**, *448*, 910–927. [CrossRef]
32. Tavecchio, F.; Maraschi, L.; Ghisellini, G. Constraints on the Physical Parameters of TeV Blazars. *Astrophys. J.* **1998**, *509*, 608–619. [CrossRef]
33. Murase, K.; Dermer, C.D.; Takami, H.; Migliori, G. Blazars as Ultra-high-energy Cosmic-ray Sources: Implications for TeV Gamma-Ray Observations. *Astrophys. J.* **2012**, *749*, 63. [CrossRef]
34. Lefa, E.; Rieger, F.M.; Aharonian, F. Formation of Very Hard Gamma-Ray Spectra of Blazars in Leptonic Models. *Astrophys. J.* **2011**, *740*, 64. [CrossRef]
35. Simet, M.; Hooper, D.; Serpico, P.D. Milky Way as a kiloparsec-scale axionscope. *Phys. Rev. D* **2008**, *77*, 063001. [CrossRef]
36. Protheroe, R.J.; Meyer, H. An infrared background-TeV gamma-ray crisis? *Phys. Lett. B* **2000**, *493*, 1–6. [CrossRef]
37. Essey, W.; Kusenko, A. A new interpretation of the gamma-ray observations of distant active galactic nuclei. *Astropart. Phys.* **2010**, *33*, 81–85. [CrossRef]
38. Essey, W.; Kalashev, O.E.; Kusenko, A.; Beacom, J.F. Secondary Photons and Neutrinos from Cosmic Rays Produced by Distant Blazars. *Phys. Rev. Lett.* **2010**, *104*, 141102. [CrossRef]
39. Essey, W.; Kalashev, O.; Kusenko, A.; Beacom, J.F. Role of Line-of-sight Cosmic-ray Interactions in Forming the Spectra of Distant Blazars in TeV Gamma Rays and High-energy Neutrinos. *Astrophys. J.* **2011**, *731*, 51. [CrossRef]
40. Zheng, Y.G.; Kang, T. Evidence for Secondary Emission as the Origin of Hard Spectra in TeV Blazars. *Astrophys. J.* **2013**, *764*, 113. [CrossRef]
41. Dong, Q.; Zheng, Y.G.; Yang, C.Y. Two components model for TeV γ -ray emission from extreme high-energy BL Lac objects. *Astrophys. Space Sci.* **2021**, *366*, 36. [CrossRef]

42. Zheng, Y.G.; Yang, C.Y.; Kang, S.J. Bethe-Heitler cascades as a plausible origin of hard spectra in distant TeV blazars. *Astron. Astrophys.* **2016**, *585*, A8. [CrossRef]
43. Kelner, S.R.; Aharonian, F.A. Energy spectra of gamma rays, electrons, and neutrinos produced at interactions of relativistic protons with low energy radiation. *Phys. Rev. D* **2008**, *78*, 034013. [CrossRef]
44. Katarzyński, K.; Sol, H.; Kus, A. The multifrequency emission of Mrk 501. From radio to TeV gamma-rays. *Astron. Astrophys.* **2001**, *367*, 809–825. [CrossRef]
45. Zheng, Y.G.; Zhang, L. Rapid TeV Flaring in Markarian 501. *Astrophys. J.* **2011**, *728*, 105. [CrossRef]
46. Mandolesi, N. Book Review: The galactic and extragalactic background radiation (IAU symposium 139)/Kluwer, 1990. *Space Sci. Rev.* **1992**, *61*, 426.
47. Ackermann, M.; Ajello, M.; Allafort, A.; Schady, P.; Baldini, L.; Ballet, J.; Barbiellini, G.; Bastieri, D.; Bellazzini, R.; Blandford, R.D.; et al. The Imprint of the Extragalactic Background Light in the Gamma-Ray Spectra of Blazars. *Science* **2012**, *338*, 1190. [CrossRef] [PubMed]
48. H. E. S. S. Collaboration; Abramowski, A.; Acero, F.; Aharonian, F.; Akhperjanian, A.G.; Anton, G.; Balenderan, S.; Balzer, A.; Barnacka, A.; Becherini, Y.; et al. Measurement of the extragalactic background light imprint on the spectra of the brightest blazars observed with H.E.S.S. *Astron. Astrophys.* **2013**, *550*, A4. [CrossRef]
49. Dwek, E.; Krennrich, F. The extragalactic background light and the gamma-ray opacity of the universe. *Astropart. Phys.* **2013**, *43*, 112–133. [CrossRef]
50. Sanchez, D.A.; Fegan, S.; Giebels, B. Evidence for a cosmological effect in γ-ray spectra of BL Lacertae. *Astron. Astrophys.* **2013**, *554*, A75. [CrossRef]
51. Dwek, E.; Krennrich, F. Simultaneous Constraints on the Spectrum of the Extragalactic Background Light and the Intrinsic TeV Spectra of Markarian 421, Markarian 501, and H1426+428. *Astrophys. J.* **2005**, *618*, 657–674. [CrossRef]
52. Mücke, A.; Engel, R.; Rachen, J.P.; Protheroe, R.J.; Stanev, T. Monte Carlo simulations of photohadronic processes in astrophysics. *Comput. Phys. Commun.* **2000**, *124*, 290–314. [CrossRef]
53. Bade, N.; Beckmann, V.; Douglas, N.G.; Barthel, P.D.; Engels, D.; Cordis, L.; Nass, P.; Voges, W. On the evolutionary behaviour of BL Lac objects. *Astron. Astrophys.* **1998**, *334*, 459–472. [CrossRef]
54. Albert, J.; Aliu, E.; Anderhub, H.; Antoranz, P.; Armada, A.; Asensio, M.; Baixeras, C.; Barrio, J.A.; Bartel, M.; Bartko, H.; et al. MAGIC Observations of Very High Energy γ-Rays from HESS J1813-178. *Astrophys. J.* **2006**, *637*, L41–L44. [CrossRef]
55. Acciari, V.A.; Aliu, E.; Arlen, T.; Beilicke, M.; Benbow, W.; Bradbury, S.M.; Buckley, J.H.; Bugaev, V.; Butt, Y.; Byrum, K.L.; et al. VERITAS Observations of the BL Lac Object 1ES 1218+304. *Astrophys. J.* **2009**, *695*, 1370–1375. [CrossRef]
56. Nolan, P.L.; Abdo, A.A.; Ackermann, M.; Ajello, M.; Allafort, A.; Antolini, E.; Atwood, W.B.; Axelsson, M.; Baldini, L.; Ballet, J.; et al. Fermi Large Area Telescope Second Source Catalog. *Astrophys. J. Suppl. Ser.* **2012**, *199*, 31. [CrossRef]
57. Acero, F.; Ackermann, M.; Ajello, M.; Albert, A.; Atwood, W.B.; Axelsson, M.; Baldini, L.; Ballet, J.; Barbiellini, G.; Bastieri, D.; et al. Fermi Large Area Telescope Third Source Catalog. *Astrophys. J. Suppl. Ser.* **2015**, *218*, 23. [CrossRef]
58. Ajello, M.; Atwood, W.B.; Baldini, L.; Ballet, J.; Barbiellini, G.; Bastieri, D.; Bellazzini, R.; Bissaldi, E.; Blandford, R.D.; Bloom, E.D.; et al. 3FHL: The Third Catalog of Hard Fermi-LAT Sources. *Astrophys. J. Suppl. Ser.* **2017**, *232*, 18. [CrossRef]
59. Sahakyan, N. Broad-band study of high-synchrotron-peaked BL Lac object 1ES 1218+304. *Mon. Not. R. Astron. Soc.* **2020**, *496*, 5518–5527. [CrossRef]
60. Condon, J.J.; Cotton, W.D.; Greisen, E.W.; Yin, Q.F.; Perley, R.A.; Taylor, G.B.; Broderick, J.J. The NRAO VLA Sky Survey. *Astron. J.* **1998**, *115*, 1693–1716. [CrossRef]
61. Giommi, P.; Polenta, G.; Lähteenmäki, A.; Thompson, D.J.; Capalbi, M.; Cutini, S.; Gasparrini, D.; González-Nuevo, J.; León-Tavares, J.; López-Caniego, M.; et al. Simultaneous Planck, Swift, and Fermi observations of X-ray and γ-ray selected blazars. *Astron. Astrophys.* **2012**, *541*, A160. [CrossRef]
62. D'Elia, V.; Perri, M.; Puccetti, S.; Capalbi, M.; Giommi, P.; Burrows, D.N.; Campana, S.; Tagliaferri, G.; Cusumano, G.; Evans, P.; et al. VizieR Online Data Catalog: 7 year Swift-XRT point source catalog (1SWXRT) (D'Elia+, 2013). *Vizier Online Data Cat.* **2013**, J/A+A/551/A142. [CrossRef]
63. Oh, K.; Koss, M.; Markwardt, C.B.; Schawinski, K.; Baumgartner, W.H.; Barthelmy, S.D.; Cenko, S.B.; Gehrels, N.; Mushotzky, R.; Petulante, A.; et al. The 105-Month Swift-BAT All-sky Hard X-Ray Survey. *Astrophys. J. Suppl. Ser.* **2018**, *235*, 4. [CrossRef]
64. Liodakis, I.; Hovatta, T.; Huppenkothen, D.; Kiehlmann, S.; Max-Moerbeck, W.; Readhead, A.C.S. Constraining the Limiting Brightness Temperature and Doppler Factors for the Largest Sample of Radio-bright Blazars. *Astrophys. J.* **2018**, *866*, 137. [CrossRef]
65. Zheng, Y.G.; Long, G.B.; Yang, C.Y.; Bai, J.M. Verification of the diffusive shock acceleration in Mrk 501. *Mon. Not. R. Astron. Soc.* **2018**, *478*, 3855–3861. [CrossRef]
66. Zheng, Y.G.; Long, G.B.; Yang, C.Y.; Bai, J.M. Formation of the Electronic Spectrum in Relativistic Jets of Gamma-Ray Blazars. *Publ. Astron. Soc. Pac.* **2018**, *130*, 083001. [CrossRef]
67. Kirk, J.G.; Dendy, R.O. Shock acceleration of cosmic rays - a critical review. *J. Phys. G Nucl. Phys.* **2001**, *27*, 1589–1595. [CrossRef]
68. Romero, G.E.; Torres, D.F.; Kaufman Bernadó, M.M.; Mirabel, I.F. Hadronic gamma-ray emission from windy microquasars. *Astron. Astrophys.* **2003**, *410*, L1–L4. [CrossRef]
69. Ackermann, M.; Ajello, M.; Allafort, A.; Baldini, L.; Ballet, J.; Barbiellini, G.; Baring, M.G.; Bastieri, D.; Bechtol, K.; Bellazzini, R.; et al. Detection of the Characteristic Pion-Decay Signature in Supernova Remnants. *Science* **2013**, *339*, 807–811. [CrossRef]

70. Padovani, P.; Resconi, E. Are both BL Lacs and pulsar wind nebulae the astrophysical counterparts of IceCube neutrino events? *Mon. Not. R. Astron. Soc.* **2014**, *443*, 474–484. [CrossRef]
71. Begelman, M.C.; Rudak, B.; Sikora, M. Consequences of Relativistic Proton Injection in Active Galactic Nuclei. *Astrophys. J.* **1990**, *362*, 38. [CrossRef]
72. Petropoulou, M.; Mastichiadis, A. Bethe-Heitler emission in BL Lacs: Filling the gap between X-rays and γ-rays. *Mon. Not. R. Astron. Soc.* **2015**, *447*, 36–48. [CrossRef]
73. Stecker, F.W. Effect of Photomeson Production by the Universal Radiation Field on High-Energy Cosmic Rays. *Phys. Rev. Lett.* **1968**, *21*, 1016–1018. [CrossRef]
74. Mücke, A.; Rachen, J.P.; Engel, R.; Protheroe, R.J.; Stanev, T. Photohadronic Processes in Astrophysical Environments. *Publ. Astron. Soc. Aust.* **1999**, *16*, 160–166. [CrossRef]
75. Sikora, M.; Stawarz, Ł.; Moderski, R.; Nalewajko, K.; Madejski, G.M. Constraining Emission Models of Luminous Blazar Sources. *Astrophys. J.* **2009**, *704*, 38–50. [CrossRef]
76. Singh, K.K.; Bisschoff, B.; van Soelen, B.; Tolamatti, A.; Marais, J.P.; Meintjes, P.J. Long-term multiwavelength view of the blazar 1ES 1218+304. *Mon. Not. R. Astron. Soc.* **2019**, *489*, 5076–5086. [CrossRef]
77. Celotti, A.; Ghisellini, G. The power of blazar jets. *Mon. Not. R. Astron. Soc.* **2008**, *385*, 283–300. [CrossRef]
78. Ghisellini, G.; Tavecchio, F.; Foschini, L.; Ghirlanda, G.; Maraschi, L.; Celotti, A. General physical properties of bright Fermi blazars. *Mon. Not. R. Astron. Soc.* **2010**, *402*, 497–518. [CrossRef]
79. Zhang, J.; Liang, E.W.; Zhang, S.N.; Bai, J.M. Radiation Mechanisms and Physical Properties of GeV-TeV BL Lac Objects. *Astrophys. J.* **2012**, *752*, 157. [CrossRef]
80. Yan, D.; Zeng, H.; Zhang, L. The physical properties of Fermi BL Lac objects jets. *Mon. Not. R. Astron. Soc.* **2014**, *439*, 2933–2942. [CrossRef]
81. Ding, N.; Zhang, X.; Xiong, D.R.; Zhang, H.J. The physical properties of Fermi TeV BL Lac objects' jets. *Mon. Not. R. Astron. Soc.* **2017**, *464*, 599–612. [CrossRef]
82. Chen, Y.; Gu, Q.; Fan, J.; Yu, X.; Zhong, X.; Liu, H.; Ding, N.; Xiong, D.; Guo, X. General Physical Properties of Fermi Blazars. *Astrophys. J. Suppl. Ser.* **2023**, *268*, 6. [CrossRef]
83. Diwan, R.; Prince, R.; Agarwal, A.; Bose, D.; Majumdar, P.; Özdönmez, A.; Chandra, S.; Khatoon, R.; Ege, E. Multiwavelength study of TeV blazar 1ES 1218+304 using gamma-ray, X-ray and optical observations. *Mon. Not. R. Astron. Soc.* **2023**, *524*, 4333–4345. [CrossRef]
84. Franceschini, A.; Rodighiero, G. The extragalactic background light revisited and the cosmic photon-photon opacity. *Astron. Astrophys.* **2017**, *603*, A34. [CrossRef]